INTERFACE

royalsocietypublishing.org/rsif

CC BY

Research

Cite this article: Gabrick EC, Batista AM, Caldas I, Kurths J, Aguiar M. 2026 Climate and dengue synchronization in southern Brazil: a municipal analysis with cross-state validation. *J. R. Soc. Interface* **23**: 20260438.
https://doi.org/10.1098/rsif.2026.0438

Received: 24 April 2026
Accepted: 19 June 2026

Subject Category:
Life Sciences–Mathematics interface

Subject Areas:
biomathematics, biophysics, environmental science

Keywords:
dengue, synchronization, climate change, vector-borne disease

Author for correspondence:
Enrique Chipicoski Gabrick
e-mail: ecgabrick@gmail.com

Climate and dengue synchronization in southern Brazil: a municipal analysis with cross-state validation

Enrique C. Gabrick[1,6], Antonio M. Batista[2,3], Iberê L. Caldas[1], Jürgen Kurths[4,5], Maíra Aguiar[6,7]

[1]Institute of Physics, University of São Paulo, São Paulo, Brazil.
[2]Graduate Program in Science, State University of Ponta Grossa, Ponta Grossa, Brazil.
[3]Department of Mathematics and Statistics, State University of Ponta Grossa, Ponta Grossa, Brazil.
[4]Potsdam Institute for Climate Impact Research, Potsdam, Germany.
[5]Department of Physics, Humboldt University Berlin, Berlin, Germany.
[6]BCAM - Basque Center for Applied Mathematics, Bilbao, Spain.
[7]Ikerbasque, Basque Foundation for Science, Bilbao, Spain.

ECG, 0000-0002-8407-7675; AMB, 0000-0002-5899-0591; ILC, 0000-0002-1748-0106; JK, 0000-0002-5926-4276; MA, 0000-0001-8354-9944

Dengue transmission is rapidly expanding beyond its historical tropical range, raising concerns about how climate change may alter the collective dynamics of epidemics. While most studies focus on transmission risk, much less is known about how climate affects the synchronization of outbreaks. In this work, we investigate dengue synchronization using epidemiological and climate data from 74 municipalities in the state of Paraná (southern Brazil) between 2010 and 2024. We quantify outbreak coherence using the event synchronization (ES) method. Our results reveal a transition from a low-transmission regime to a high-transmission regime accompanied by a marked increase in synchronization across cities. We also show that climate anomalies increase the number of permissive days for dengue transmission. Our results suggest that such days are significantly associated with outbreak synchronization. We identify a two-stage climate mechanism: conducive climatic conditions first reduce the probability of asynchronous states and coincide with the emergence of synchronized outbreaks, and subsequently sustain higher synchronization levels. Extending the analysis through comparative analyses in Ceará and Minas Gerais, we uncover that climate consistently amplifies synchronization, although its role in the onset of synchronization depends on regional climatic regimes. These findings highlight climate-driven synchronization as an emerging feature shaping dengue dynamics.

1. Introduction

Transmitted by *Aedes aegypti* and *Aedes albopictus* mosquitoes, dengue now threatens about half of the world's population, with an estimated 100–400 million infections each year [1,2]. Dengue is caused by four distinct viral serotypes (DENV-1 to DENV-4) and is spread to humans through the bites of infected mosquitoes [3]. Most cases are asymptomatic or mild, and infected individuals typically recover within one to two weeks. However, the immune response to dengue is complex [4]. Infection with one serotype provides long-term immunity to that serotype and temporary cross-protection against the others [5]. Once this cross-protection wanes, subsequent infections with a different serotype increase the risk of severe dengue, which can be fatal [6]. However, recent

© 2026 The Authors. Published by the Royal Society under the terms of the Creative Commons Attribution License http://creativecommons.org/licenses/by/4.0/, which permits unrestricted use, provided the original author and source are credited.

THE ROYAL SOCIETY PUBLISHING

Downloaded from royalsocietypublishing.org/rsif/article-pdf/doi/10.1098/rsif.2026.0438/6159915/rsif.2026.0438.pdf
by guest
on 05 November 2026

findings suggest that complete lifelong protection against the same serotype may not always hold, highlighting the need to reconsider dengue immunity and reinfection dynamics [7,8].

Mathematical modelling has been central to dengue research, providing insight into how multi-serotype transmission, temporary cross-immunity, antibody-dependent enhancement, vaccination, vector dynamics and control interventions shape epidemic behaviour. Previous models have shown that dengue can generate complex nonlinear dynamics, including oscillations, bifurcations, chaotic behaviour and sensitivity to data quality and parameter estimation [9–14]. Other studies have examined dengue vaccination, serotype-specific cross-protection and the interpretation of vaccine trials and public-health interventions [15–17]. More recent modelling frameworks have extended these approaches to explicit vector dynamics and behavioural or control mechanisms, highlighting the importance of integrating biological, epidemiological and environmental processes in dengue models [18,19].

Because dengue transmission depends on the interaction between host immunity, mosquito ecology and environmental suitability, understanding the climatic sensitivity of the vector is essential [20,21]. Mosquitoes are directly affected by climate and environmental conditions [22–24]. Temperature substantially modulates dengue transmission by regulating mosquito development, survival, biting rates and the virus's extrinsic incubation period [25]. These features respond strongly to temperature and are amplified within the range 18–34°C for *A. aegypti* and *A. albopictus*. However, the optimal efficiency remains within a narrower range [26]. On the other hand, precipitation exerts a more complex and nonlinear influence on vector abundance [27,28]. Moderate rainfall regimes generally increase vector abundance by increasing the availability of breeding sites, whereas extreme rainfall can lead to flushing effects, as observed in Singapore [29]. Paradoxically, drought periods can also increase vector abundance, because drought can lead households to store water, which can create additional breeding sites [30]. Owing to the environmental conditions required for mosquito development and survival, dengue was historically confined to tropical and subtropical regions [2]. However, recent studies indicate that climate change and other anthropogenic factors have contributed to the geographic expansion of dengue transmission risk beyond these regions [31–36]. This expansion is increasingly relevant in temperate settings, where invasive mosquitoes are becoming established [37–39] and climate-based forecasting approaches have highlighted the role of temperature, precipitation and humidity in shaping mosquito abundance and local transmission potential [40]. Climate change is one of the main factors linked to the changing geographical range of dengue and other infectious diseases [41,42]. By altering vector distributions, behaviour and density, favourable climatic conditions can contribute to outbreaks in previously unaffected regions, including dengue and chikungunya outbreaks in Europe [43–45]. Nevertheless, excessive warming driven by climate change may exceed the upper thermal limits of mosquitoes, consequently reducing the transmission potential of vector-borne diseases, as observed in North Africa [46]. In addition to the role of climate, human mobility also plays a key role in the spread of vectors and pathogens across regions [47]. Although the expansion of dengue transmission risk under climate change has been widely studied [48–51], much less is known about how climate variability affects the collective spatio-temporal dynamics of dengue outbreaks across regions.

Understanding collective epidemic patterns requires tools capable of quantifying coordinated dynamics between locations. One such approach is the use of synchronization metrics, which are widely employed in several fields where oscillating systems adjust their rhythms [52]. In epidemiological systems, synchronization provides a natural framework to quantify the coherence of outbreaks across spatially separated regions [53]. Analysing dengue surveillance data from 14 countries across the Americas, Johansson *et al.* reported strong synchronization of dengue dynamics at both seasonal and multi-annual time scales. Large epidemics at multi-annual scales were shared across the region, with an average temporal lag of only six months even between locations separated by distances of up to 10 000 km. The authors also showed that seasonal synchrony is associated with climatic variables, including temperature, rainfall and El Niño Southern Oscillation [54]. Similar region-wide synchrony and travelling-wave behaviour have also been documented across Southeast Asia, where elevated temperatures were linked to synchronous dengue epidemics [55]. Results from Thailand similarly indicate that dengue synchrony is related to temperature patterns: periods of strong synchronization coincide with coherent temperature fluctuations, whereas multi-annual oscillations associated with population immunity can generate asynchronous dynamics [56,57]. Under such conditions, temperature synchrony can act as an external driver capable of re-synchronizing dengue epidemics across regions [56]. In Brazil, dengue epidemics exhibit a clear spatio-temporal structure, with travelling waves typically starting in the western states and propagating eastwards. Consistent with this spatial propagation, epidemic synchrony decreases with increasing geographical distance between regions. These spatial patterns are shaped by a combination of human mobility, supported by gravity-style models, and climate factors [58]. Although dengue synchrony has been linked to climate variability in several regions worldwide, much less is known about synchronization among cities in Brazil, one of the countries most heavily affected by dengue. In this work, we investigate how dengue synchronization is modulated by climatic factors, particularly temperature and precipitation. Although synchronization in epidemic systems has been extensively studied [59–62], most existing approaches rely on wavelet-based methods [54,56] or pairwise correlation analyses [58]. Here, we quantify outbreak synchronization using an adaptation of the nonlinear event synchronization (ES) method [63,64], a framework for measuring the temporal alignment of discrete events, such as rainfall. ES has been widely employed to quantify nonlinear interdependence in complex systems, with applications in neuroscience [65,66] and climate science [67–69]. To the best of our knowledge, this method has not yet been systematically applied to characterize synchronization in epidemic outbreaks. Its application, therefore, represents a novel methodological contribution to the study of infectious disease dynamics. Through this method, we characterize outbreak synchronization among municipalities in southern Brazil and, based on regression analysis, we show that the connections shaping synchronization behaviour are mediated by climatic conditions.

This paper is organized as follows. In §2, we describe the epidemiological and climatic datasets together with the ES methodology. Section 3 presents evidence of a phase transition associated with the geographical expansion of dengue transmission. In §4, we analyse the spatio-temporal synchronization patterns of dengue outbreaks. Section 5 investigates how climatic anomalies

Downloaded from royalsocietypublishing.org/rsif/article-pdf/doi/10.1098/rsif.2026.0438/6159915/rsif.2026.0438.pdf
by guest
on 05 November 2026

modify the number of climate-permissive transmission days, and how these variables relate to synchronization dynamics. In §6, we extend the analysis to two additional Brazilian states to evaluate the generality of the proposed pattern. In §7, we perform a sensitivity analysis of the synchronization window and outbreak threshold. Finally, §8 summarizes the main findings and discusses their epidemiological implications.

2. Methodology

2.1. Dengue data

In this work, we use notified dengue case data from the InfoDengue platform [70], an early-warning surveillance system that compiles arboviral (dengue, chikungunya and Zika) case notifications for all Brazilian municipalities. The platform integrates epidemiological, climatic and demographic information from multiple official sources and applies statistical and nowcasting procedures to correct reporting delays, generating a harmonized dataset with weekly resolution.

We analysed weekly dengue notifications from the first epidemiological week of 2010 to the last epidemiological week of 2024 (3 January 2010 to 22 December 2024), comprising 782 consecutive weeks. The dataset provides notified cases but does not include detailed serological confirmation data, as only a fraction of reported cases are laboratory-confirmed in Brazil. To describe the co-circulation of dengue virus serotypes over time, we obtained the data from the official state epidemiological reports [71].

Brazil is endemic for dengue and accounts for a substantial proportion of global cases annually. While the highest historical burden has been concentrated in the North, Northeast, Central-West and Southeast regions, southern states have traditionally reported lower incidence. However, they exhibit marked intra-state heterogeneity, with some municipalities classified as endemic and others presenting sporadic transmission. Paraná represents a paradigmatic example of this transitional epidemiological setting.

Paraná is characterized by pronounced climatic heterogeneity. The southern region has a temperate subtropical climate with cooler winters and mean summer temperatures below 22°C, whereas the northern and northwestern regions present warmer subtropical conditions, with mean summer temperatures exceeding 22°C. The coastal area exhibits a humid tropical climate. Together with socioeconomic differences and population distribution across the 399 municipalities, there is substantial spatial variability in the incidence of dengue in Paraná.

Municipal population sizes range from approximately 1300 to 1.9 million inhabitants (IBGE census data from 2022 [72]). To reduce stochastic effects associated with very small populations and sporadic reporting, we applied two inclusion criteria: (i) municipalities with more than 20 000 inhabitants and (ii) municipalities reporting more than 1000 cumulative dengue cases over the study period (2010–2024). After applying these filters, 74 municipalities were retained for our analysis, ensuring representation from all geographic regions of Paraná.

Although demographic data are available through InfoDengue, we used official population estimates from the 2022 Brazilian national census (IBGE) to use a single demographic census [72].

In addition, we ordered the municipalities by latitude and assigned a numerical index (IDX= $1, 2, \ldots, 74$).

2.2. Climate data

Although InfoDengue provides weekly climate indicators (e.g. mean temperature and humidity), these variables contain missing values for several municipalities in our dataset. To ensure spatial completeness and to construct a consistent historical baseline, we used the ERA5-L and reanalysis dataset [73]. The dataset provides hourly surface climate variables with a horizontal resolution of $0.1° \times 0.1°$ (native resolution of 9 km), which is adequate for a municipality-level analysis.

For each municipality, we extracted the daily near-surface air temperature and total precipitation from 1 January 1980 to 28 December 2024. Municipal boundaries were obtained from the official 2024 Brazilian municipal grid provided by IBGE [74]. Gridded climate data were spatially aggregated within each municipal boundary. Daily values were subsequently aggregated to weekly or monthly resolution when required for the analysis.

To quantify climate anomalies, we divided the dataset into a historical baseline period (1 January 1980 to 2 January 2010) and a study period (3 January 2010 to 28 December 2024). For temperature (T, in °C) and precipitation (P, in mm), we computed the historical climatological mean for each month and municipality, denoted by $\overline{x}^{\text{hist}}_{m,i}$, where $x \in \{T, P\}$, m denotes the month and i denotes the municipality index. Then, we calculated the monthly anomalies, defined as deviations from the historical climatological reference, through

$$x^{an.}_{m,i} = x_{m,i} - \overline{x}^{\text{hist.}}_{m,i}, \tag{2.1}$$

where $x_{m,i}$ represents the observed monthly mean temperature or accumulated precipitation for municipality i in month m during the study period. Positive values indicate warmer or wetter conditions relative to the reference interval (1980–2010).

2.3. Synchronization metric

To quantify the temporal alignment of dengue outbreaks across municipalities, we employed the ES method [63,64], which measures the temporal coincidence of discrete events within a predefined tolerance window [75]. ES is a robust metric that can be

Downloaded from royalsocietypublishing.org/rsif/article-pdf/doi/10.1098/rsif.2026.0438/6159915/rsif.2026.0438.pdf
by guest
on 05 November 2026

employed for time series characterized by intermittency, non-Gaussian distributions and outbreak-like dynamics [68]. This makes the method suitable for epidemic time series.

For each municipality i, outbreak events are identified from the weekly dengue case time series $c_i(t)$. First, we computed the mean weekly incidence over the entire study period, denoted by $\bar{c}_i$. An outbreak episode is defined as a period during which $c_i(t) \geq \bar{c}_i + 1$, beginning when $c_i(t)$ crossed above this threshold. The episode is considered terminated when the time series remains below this threshold for at least two consecutive weeks, preventing short-term fluctuations from being classified as separate outbreaks.

Within each outbreak interval $[t_{\text{start}}, t_{\text{end}}]$, we defined a single event corresponding to the week of maximum incidence, according to

$$t_k^i = \arg\max_{t \in [t_{\text{start}}, t_{\text{end}}]} c_i(t), \tag{2.2}$$

where t_k^i represents the timing of the kth outbreak peak in municipality i. Each outbreak interval, therefore, contributed one discrete event. The full set of outbreak peaks for municipality i is given by $\{t_k^i\}_{k=1}^{N_i}$, where N_i denotes the total number of outbreaks identified during the study period. Municipalities that reported at least one event in a given period of time are referred to as active cities.

For two municipalities x and y, with event series $\{t_k^x\}_{k=1}^{N_x}$ and $\{t_j^y\}_{j=1}^{N_y}$, respectively, two outbreak peaks were considered temporally synchronized when their occurrence times differed by at most a tolerance window τ, that is,

$$|t_k^x - t_j^y| \leq \tau. \tag{2.3}$$

Throughout this study, we adopted $\tau = 2$ weeks. In our datasets, outbreak durations have a mean of 11 weeks (25th–75th percentile: 2–16 weeks). The adopted tolerance window is substantially shorter than the characteristic outbreak duration observed in the data, making the synchronization criterion conservative and focused on near-coincident epidemic peaks while excluding outbreaks that merely overlap in time.

To characterize synchronization at the state level, we constructed a weekly synchronization index Syn(t). For each municipality i and week t, we defined

$$E_i(t) = \begin{cases} 1, & \text{if an event occurs in } [\,t - \tau,\ t + \tau\,], \\ 0, & \text{otherwise.} \end{cases} \tag{2.4}$$

Then, Syn(t) is

$$\text{Syn}(t) = \begin{cases} \frac{1}{N} \sum_{i=1}^{N} E_i(t), & \text{if } \sum_{i=1}^{N} E_i(t) > 1, \\ 0, & \text{otherwise,} \end{cases} \tag{2.5}$$

where N is the total number of municipalities and $\text{Syn}(t) \in [0, 1]$.

Therefore, Syn(t) represents the fraction of municipalities experiencing outbreak peaks within a ±2-week window centred at week t. Low values of Syn(t) indicate temporally localized transmission restricted to a small number of municipalities, whereas high values reflect concurrent outbreaks across a large portion of the state. In this framework, synchronization captures the degree of regional epidemic coherence rather than simply the magnitude of incidence.

As an illustrative example, figure 1*a*,*b* displays weekly dengue incidence for two municipalities. In each panel, the magenta horizontal dotted line represents the long-term mean incidence ($\bar{c}_i$). An outbreak episode is defined as occurring when the time series crosses above this threshold; upward and downward crossings are indicated by open circles. This defines the outbreak interval $[t_{\text{start}}, t_{\text{end}}]$. Within each interval, the week of maximum incidence (black dot) is identified and defined as the outbreak event. For instance, in panel (a), the first outbreak peak occurs in epidemiological week 14 of 2013, while in panel (b), the corresponding peak occurs in week 12 of 2013. Given a tolerance window of $\tau = \pm 2$ weeks, these two peaks are regarded as temporally synchronized. While this example illustrates synchronization between a pair of municipalities, the synchronization index defined in equation (2.5) generalizes this procedure to N municipalities simultaneously, providing a state-level measure of outbreak alignment.

2.4. Break point detection

To identify potential structural changes in the long-term dengue dynamics, we analysed the cumulative number of aggregated notified dengue cases across all municipalities. We applied a change-point detection procedure using the dynamic programming algorithm implemented in the *ruptures* package [76]. This method partitions the time series into segments by minimizing a global cost function, while ensuring the optimal segmentation for a predefined number of break points. Here, we searched for a single break point. We adopted the radial basis function cost model, which is sensitive to changes in the statistical properties of the signal, including changes in trend and growth regime. The estimated change-point occurred on 19 January 2020. This break point was subsequently used to define the pre- and post-transition periods employed throughout our study. In addition, to characterize

Downloaded from royalsocietypublishing.org/rsif/article-pdf/doi/10.1098/rsif.2026.0438/6159915/rsif.2026.0438.pdf
by guest
on 05 November 2026

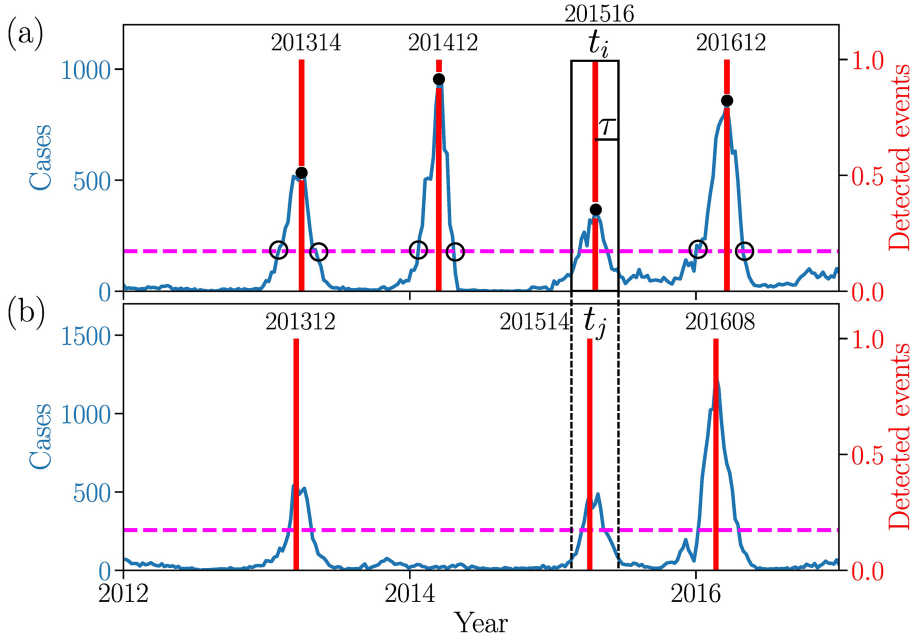


Figure 1. Illustration of outbreak detection and ES for two municipalities: (a) Maringá and (b) Foz do Iguaçu. The blue curves represent weekly dengue cases, while the magenta dashed line denotes the long-term mean incidence used as the outbreak threshold (2010–2024). Open circles indicate threshold crossings that define outbreak intervals, black dots mark the outbreak peaks and red vertical bars represent the detected events. The shaded region illustrates the tolerance window τ around an event. Peaks occurring within a $\pm$2-week interval are considered temporally synchronized.

dynamical differences between the two regimes, we fitted power-law functions to the cumulative incidence before and after the detected break point.

3. Phase transition and geographical expansion of dengue

The notified dengue cases in Paraná display a clear temporal shift in the number of cases, where the reported cases before 2020 remain below the historical average number of cases plus one standard deviation (figure 2*a*, blue curve). This transition is particularly evident in the cumulative time series (red curve in figure 2*a*), which reveals a sharp change in power-law behaviour, suggesting a change-point at 19 January 2020 (vertical dotted lime line in figure 2*a*). Before this break point, the cumulative incidence grows as $t^{0.940(7)}$, whereas after it accelerates sharply, proportional to $t^{2.79(5)}$. The break point is interpreted as a statistical change-point in dengue incidence rather than as the direct manifestation of a single biological mechanism, and it marks an increase in the incidence regime. Therefore, the break point is not defined by a specific biological threshold, but by an abrupt change in the epidemiological dynamics observed in the surveillance data. Several factors may contribute to this transition, including improvements in disease surveillance, which probably increased case detection, serotype circulation [20], human behaviour and climate conditions. However, these factors alone do not readily explain the magnitude and spatial coherence of the observed increase, which extends beyond southern Brazil and is also observed in Latin America [77]. Furthermore, serotype co-circulation alone is not sufficient to explain the observed transition, because DENV-1, DENV-2 and DENV-3 co-circulated for most of the study period, with episodic reintroductions of DENV-4 in 2016, 2023 and 2024, as shown in the upper panel of figure 2*a*. Notably, the largest outbreaks (2023 and 2024) coincide with DENV-4 reintroduction; nevertheless, serotype turnover alone does not account for the abrupt change in the scaling regime. Human behaviour is difficult to quantify and relevant data are lacking; therefore, it is not investigated here. By contrast, climate conditions have been identified as an important factor in the expansion of dengue across different localities [51,78], and may help explain this abrupt transition. Together, these results suggest that the observed transition reflects a substantial change in transmission conditions, pointing to additional large-scale drivers, including climate variability and geographical expansion, as plausible contributors to the recent acceleration of dengue incidence.

The spatial patterns reveal a marked geographical expansion of dengue incidence, with cities previously unaffected, or reporting only a few cases, beginning to register cases after the break point (figure 2*b*). Before the break point, most cities exhibit predominantly blue tones, with only localized white bands, mainly in northern municipalities. A first large-scale outbreak occurred in 2016, representing the most intense event up to that year, and affected practically all the considered cities. Following this event, a marked reduction in reported cases is observed in both figure 2*a*,*b*, which may reflect partial population immunity. Despite this, a sharp resurgence of dengue occurred after 2020. In the post-break point period, figure 2*b* displays widespread white and red regions, indicating large positive deviations from historical means. After 2022, several southern cities exhibited intense outbreaks, culminating in a geographical expansion together with an unprecedented, in the considered period, increase in reported cases, which explains the extreme peak observed in that year. Relative to historical variability, 2024 represents an extreme event, with

Downloaded from royalsocietypublishing.org/rsif/article-pdf/doi/10.1098/rsif.2026.0438/6159915/rsif.2026.0438.pdf
by guest
on 05 November 2026

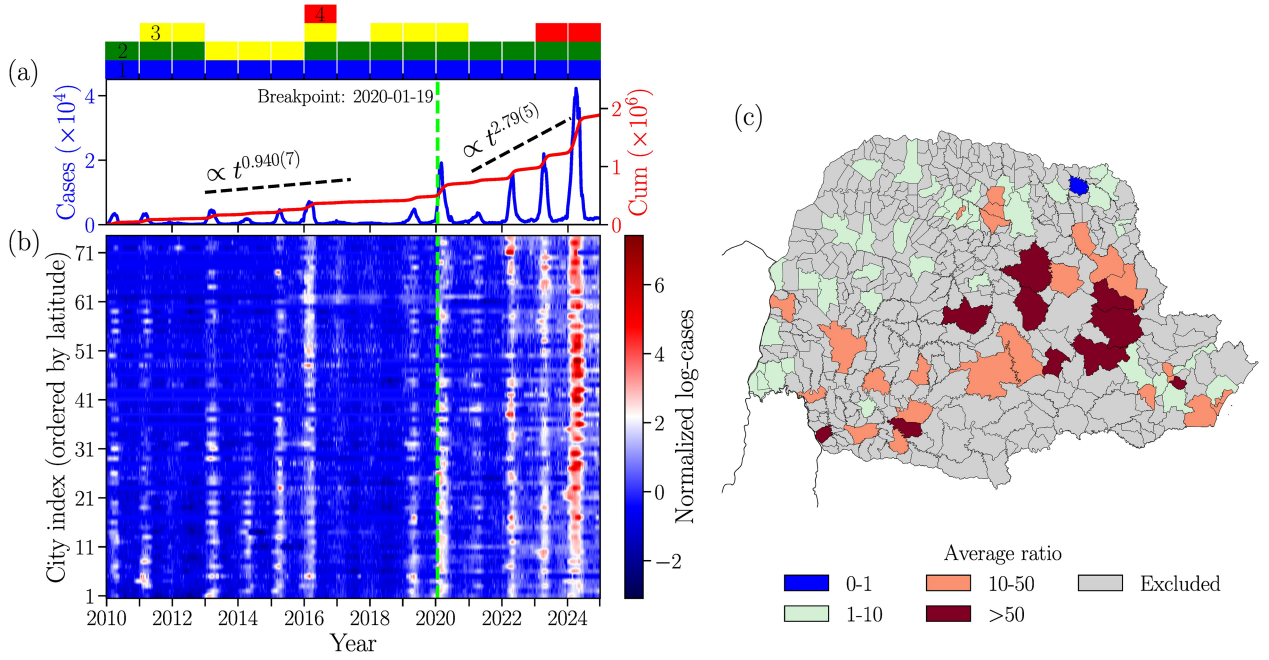


Figure 2. (a) Weekly notified dengue cases (blue curve) and cumulative cases (red curve). The serotype circulation in each year is displayed by the coloured blocks above panel (a), where the presence of DENV-1, 2, 3 and 4 is represented by blue, green, yellow and red blocks, respectively. The lime vertical dashed line marks the estimated break point (19 January 2020). Before and after the break point, the cumulative curve follows different scaling regimes, growing as $t^{0.940(7)}$ and $t^{2.79(5)}$, respectively. (b) Heatmap of normalized dengue cases by year and city index (ordered by latitude). Red and white tones indicate large positive deviations from the mean logarithmic number of cases, whereas blue tones indicate reductions. The normalization is defined as Norm. Cases $= (\text{cases}_{\log} - \overline{\text{cases}_{\log}})/\sigma(\text{cases}_{\log})$, with $\text{cases}_{\log} = \log(\text{cases} + 1)$. (c) Map of Paraná shows the ratio between the average weekly number of dengue cases before and after the break point; excluded municipalities are shown in grey.

deviations exceeding seven standard deviations of the local time series. This spatial expansion substantially increases the burden on public health systems, as dengue transmission now affects cities that were previously unexposed.

By comparing the average weekly dengue cases before and after the break point for each city, we observe a pronounced increase in incidence in almost all municipalities (figure 2*c*), with some cities exhibiting increases exceeding a factor of 50. These extreme ratios arise primarily because several cities were previously unaffected or reported only sporadic cases, resulting in near-zero average incidence before 2020. The most pronounced increases are concentrated in central-eastern municipalities. Beyond these critical areas, almost all cities display post-break point ratios greater than unity, indicating a generalized rise in dengue transmission. Only one municipality exhibits a ratio between 0 and 1 (blue), which is associated with a highly noisy time series. Together, the patterns shown in figure 2*b*,*c* indicate that previous geographical limits of dengue transmission have been crossed, with all analysed cities now reporting cases. Notably, the year 2024 exhibits a continuous red band in figure 2*b*, suggesting large-scale synchronization of outbreaks across the state.

The widespread spatial expansion and the emergence of nearly simultaneous outbreaks across municipalities suggest that dengue dynamics in Paraná are increasingly consistent with the influence of common external forcing, rather than isolated local processes.

4. Spatio-temporal synchronization of dengue outbreaks

The spatial diffusion of dengue incidence and the progressive reduction of local heterogeneities motivate the analysis of spatio-temporal synchronization as a defining feature of the post-break point regime. As dengue expands geographically across the state, outbreaks that were previously asynchronous increasingly align in time, indicating a transition towards a more coherent dynamical regime.

Employing the ES metric, we find that the synchronization signal closely follows the fraction of dengue cases, as shown by the black and dotted blue curves, respectively, in figure 3*a*. Synchronization peaks systematically coincide with peaks in incidence, resulting in a high correlation between the two signals (Spearman $\rho = 0.80$ and Pearson $r = 0.68$). Overall, major outbreaks are characterized by elevated synchronization levels, with the notable exception of the 2024 outbreak. High peaks in the synchronization and fraction of cases indicate that large epidemics emerge from the quasi-simultaneous activation of multiple cities.

Years with high synchronization levels correspond to periods with a larger number of active cities (e.g. 2016, 2020, 2022 and 2023), whereas synchronization collapses when only a few municipalities report cases. Notably, 2012, 2017 and 2018 mark minima in the number of active cities and, consequently, in synchronization levels. The latter two years coincide with the period following

Downloaded from royalsocietypublishing.org/rsif/article-pdf/doi/10.1098/rsif.2026.0438/6159915/rsif.2026.0438.pdf
by guest
on 05 November 2026

the vaccination campaign initiated in 2016, which is not explored here. Therefore, the number of cities reporting outbreaks provides essential context for interpreting the synchronization signal, as shown in figure 3*a*. This interpretation is supported by figure 3*b*.

Together, the information from figure 3*a,b* reveals four distinct synchronization regimes. (i) Between 2010 and 2016, we observe few cities reporting events in 2010, 2011, 2012 and 2014, with low levels of synchronization and low interquartile ranges (IQR; black squares in figure 3b). In particular, 2012 shows practically null cases and synchronization. On the other hand, 2013, 2015 and 2016 exhibit increases in mean synchronization levels and IQR. In particular, 2016 shows a distinct regime compared with previous years, with around 60 active cities, high average synchronization, and high IQR.

(ii) This regime collapses in 2017–2018, when synchronization sharply decreases alongside a reduction in the number of active cities, reflecting the combined effects of epidemiological control and accumulated immunity. Compared with 2017 and 2018, the number of active cities began to increase again after 2019. Overall, the pre-break point regimes ((i) and (ii)) are characterized by limited spatial activation and synchronization constrained to a relatively fixed subset of cities.

(iii) After 2020, synchronization increases again, driven by a substantial rise in the number of active cities, except for 2021, which was strongly affected by the COVID-19 pandemic and disruptions in public health services. Up to 2023, the number of active cities, the fraction of cases and the synchronization level remain strongly correlated, as evidenced by the signals in figure 3*a,b*. (iv) By contrast, the 2024 outbreak exhibits a qualitatively different behaviour: although incidence reaches historically high levels, the maximum synchronization peak is lower than in previous years (e.g. 2023). At the same time, 2024 presents the highest annual mean synchronization and variability (IQR = 0.21). Unlike earlier outbreaks, synchronization in 2024 is no longer dominated by a single, temporally coherent event. Instead, multiple outbreak waves occur throughout the year across all cities, sustaining synchronization over an extended period. This pattern indicates a distinct synchronization regime, characterized by stronger temporal heterogeneity and overlapping epidemic waves.

This shift is further reflected in the seasonal distribution of outbreaks. Figure 3*c* shows the number of cities reporting at least one outbreak event per month before and after the break point (blue and orange bars, respectively). In the pre-break point regime, dengue activity is largely confined to the first five months of the year, whereas the post-break point period exhibits a broader and temporally shifted activation pattern. Before the break point, outbreaks peak in April, consistent with the historical seasonal cycle of temperature and precipitation. By contrast, after the break point, outbreaks emerge earlier and persist later into the year, involving a substantially larger number of cities. This seasonal shift suggests a change in the climatic forcing acting on dengue transmission. Remarkably, sporadic outbreaks are now observed during winter months, when historical mean temperatures are below 20°C.

Overall, our results indicate that dengue synchronization in Paraná has transitioned from a temporally and spatially constrained regime, characterized by well-defined seasons and a limited set of endemic cities, to a more dispersed and persistent state, in which transmission involves newly exposed cities and extended activity periods. This transition is consistent with changes in climatic forcing and seasonality acting coherently across space.

5. Climate anomalies, permissive transmission days and synchronization

As described above, dengue transmission in Paraná has undergone substantial changes in recent years, including a marked geographical expansion into previously unaffected less-affected cities. Dengue dynamics is strongly constrained by environmental conditions that modulate the mosquito life cycle. Consequently, the number of days with climatically permissive conditions acts as an effective control parameter for transmission intensity. In this section, we show that anomalous weather conditions have substantially increased the number of conducive days, amplifying epidemic risk across the state.

Paraná exhibits four well-defined seasons, with monthly mean temperatures ranging from 15.85°C in July to 23.39°C in January (figure 4*a*), and the rainy season starting from September to March, including spring and summer months (figure 4*c*). This seasonal regime has historically confined dengue transmission to specific regions and periods of the year.

This historical climate pattern has been progressively modified by climate anomalies, as shown in figure 4*b,d* for temperature and precipitation, respectively. Temperature anomalies exhibit an increasing trend, particularly after 2017, with September showing the largest positive deviations. Furthermore, the years 2023 and 2024 are the warmest across almost all months, coinciding with the period of most intense dengue activity.

These thermal anomalies, together with the increase in temperatures observed since 2020, are consistent with the observed shift in the timing of outbreak events (figure 3*c*). Remarkably, 2024 is the year with record temperatures and dengue incidence, supporting the role of temperature as a key factor in dengue transmission.

Comparing these climatic characteristics with the four synchronization regimes identified in §4, we find that regimes (iii) and (iv), the most active ones, coincide with high temperature anomalies (figure 4*b*) and anomalies in rainfall patterns (figure 4*d*).

Precipitation patterns also show substantial deviations from their historical monthly means. While some months exhibit reduced rainfall (negative anomalies), others experience extreme rainfall events (figure 4*d*), indicating a reorganization of hydrological regimes across the state. By contrast to temperature, precipitation anomalies do not display a sustained increasing trend. Together, these results suggest a shift towards hotter conditions across most months, accompanied by more variable rainfall regimes, including both drought and extreme precipitation events.

Downloaded from royalsocietypublishing.org/rsif/article-pdf/doi/10.1098/rsif.2026.0438/6159915/rsif.2026.0438.pdf
by guest
on 05 November 2026

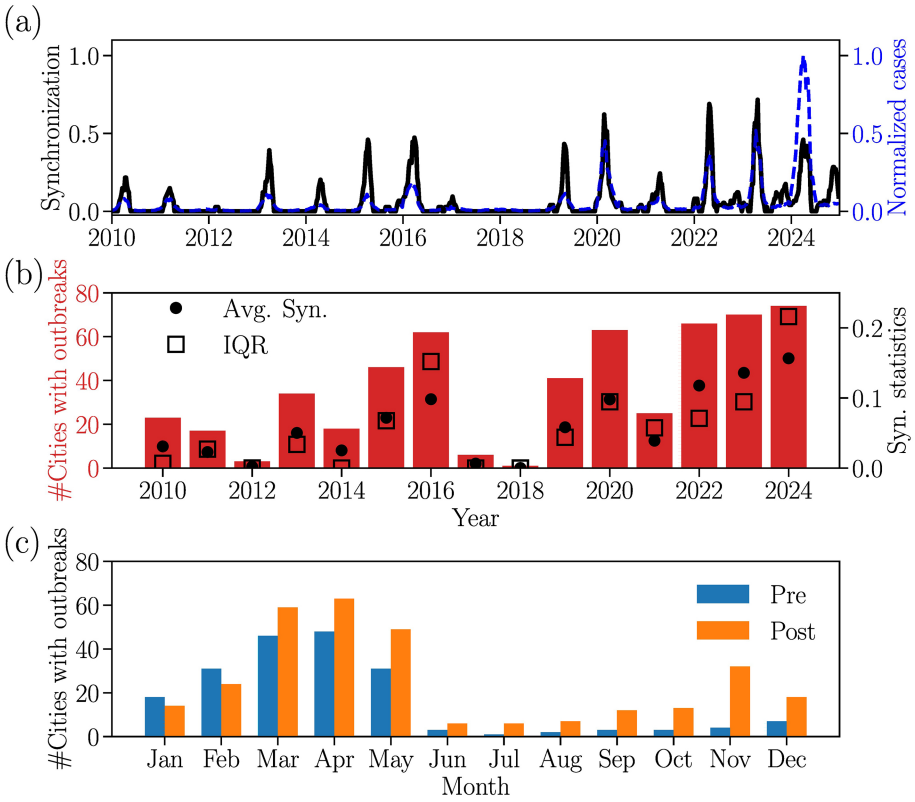


Figure 3. (a) Weekly synchronization (black curve) and fraction of dengue cases (blue dashed curve). (b) Red bars indicate the number of cities reporting at least one outbreak event per year, while black circles and open squares show the annual mean synchronization and IQR, respectively. (c) Number of cities reporting at least one outbreak event per month before and after the break point shown by the blue and orange bars, respectively.

5.1. Anomalous temperature increases the number of thermal optimal days

We define thermally possible days for transmission as those with temperatures between 18 and 34°C, and thermally optimal days as those with temperatures between 26 and 29°C [25,26]. Based on these thresholds, we computed the monthly number of thermally permissive days for each city. Here, thermally permissive days refer to the combined set of possible and optimal thermal days. By computing the correlation between thermally possible and optimal days, we obtain an average value across all municipalities of 0.44. However, this correlation varies substantially across municipalities, ranging from 0.02 in Prudentópolis to 0.74 in Foz do Iguaçu. These results indicate that, although the two variables are related, the degree of association is moderate on average and spatially heterogeneous; therefore, we retained both variables in the multiple model. We then estimated the Pearson correlation between local temperature anomalies and the number of conducive thermal days. Averaged across the 74 cities, temperature anomalies exhibit a positive correlation with both optimal days ($r = 0.39$ and $p = 0.01$) and possible days ($r = 0.26$ and $p = 0.003$). These results indicate that temperature anomalies are associated with an increase in the number of thermally favourable days. Although the relationship includes nonlinear components, a substantial linear component is still evident; therefore, we used linear regression to measure the effect of temperature anomaly on permissive days.

For each municipality, we fitted a linear regression of the form

$$y_t^i = \beta_0^i + \beta_1^i \,\text{anomaly}_t^i + \epsilon_t^i, \tag{5.1}$$

where $i \in [1, 74]$ denotes the municipality index, y_t^i is the number of optimal or possible days per month, $\beta_{0,1}^i$ are regression coefficients and ϵ_t^i represents random variability. When $\beta_1^i > 0$ and $p < 0.05$, we interpret this as evidence of a positive association between temperature anomaly and thermally permissive days. Figure 5*a–d* displays the regression coefficients for optimal and possible days, respectively. In both panels, the error bars indicate 95% confidence intervals for β_1^i. For simplicity, we denote these coefficients by β_{opt} and β_{poss}.

For northern cities (index 1 to 39), the number of thermally optimal days systematically increased with temperature anomaly (figure 5*a,b*). By contrast, southern municipalities display more heterogeneous responses, with many coefficients close to or equal to zero. Notably, several cities with $\beta_{\text{opt}} \sim 0$ belong to a region that was strongly affected by dengue after 2020, as shown in figure 3*c*. This apparent divergence suggests that optimal thermal conditions alone are not sufficient to explain recent outbreaks.

When the regression is performed with y_t^i defined as the number of possible days, the results, shown in figure 5*c,d*, reveal a consistent and statistically significant increase in β_{poss} across all considered cities. Remarkably, β_{poss} approximately increases across municipalities as we advance along the city index, suggesting that temperature anomalies are expanding the number of possible

Downloaded from royalsocietypublishing.org/rsif/article-pdf/doi/10.1098/rsif.2026.0438/6159915/rsif.2026.0438.pdf
by guest
on 05 November 2026

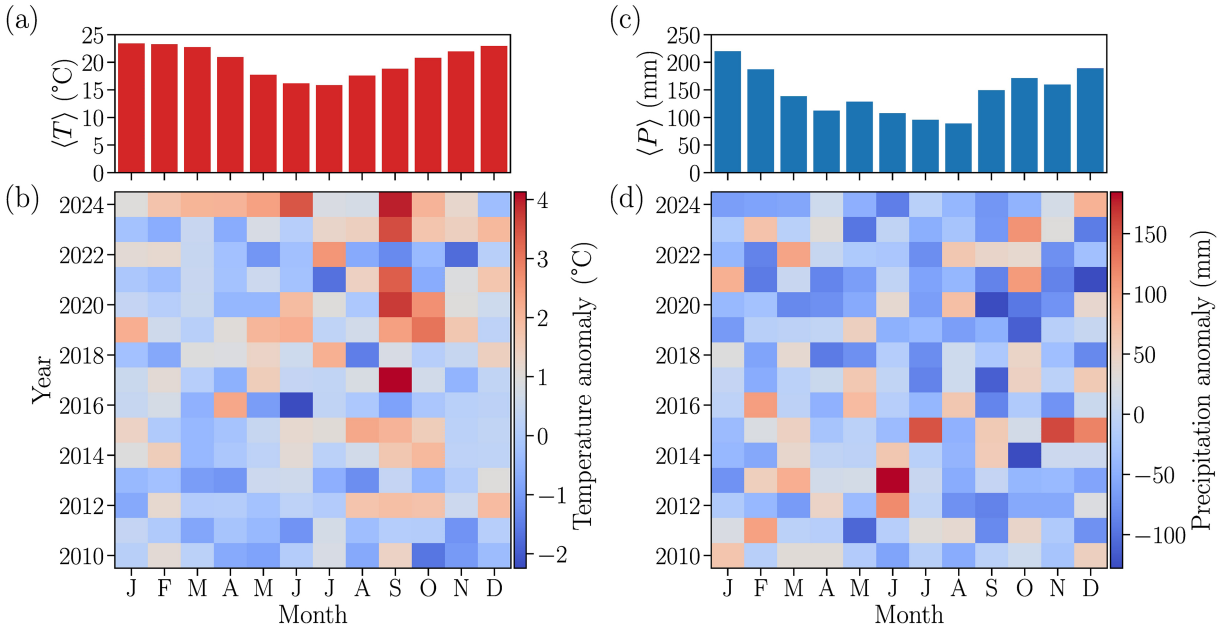


Figure 4. Panels (a) and (c) show the historical monthly mean temperature and precipitation in Paraná, respectively, based on the reference period 1 January 1980 to 2 January 2010. The notation $\langle \cdot \rangle$ means the spatial average across all considered municipalities. Panels (b) and (d) show the corresponding monthly temperature and precipitation anomalies during the study period, respectively.

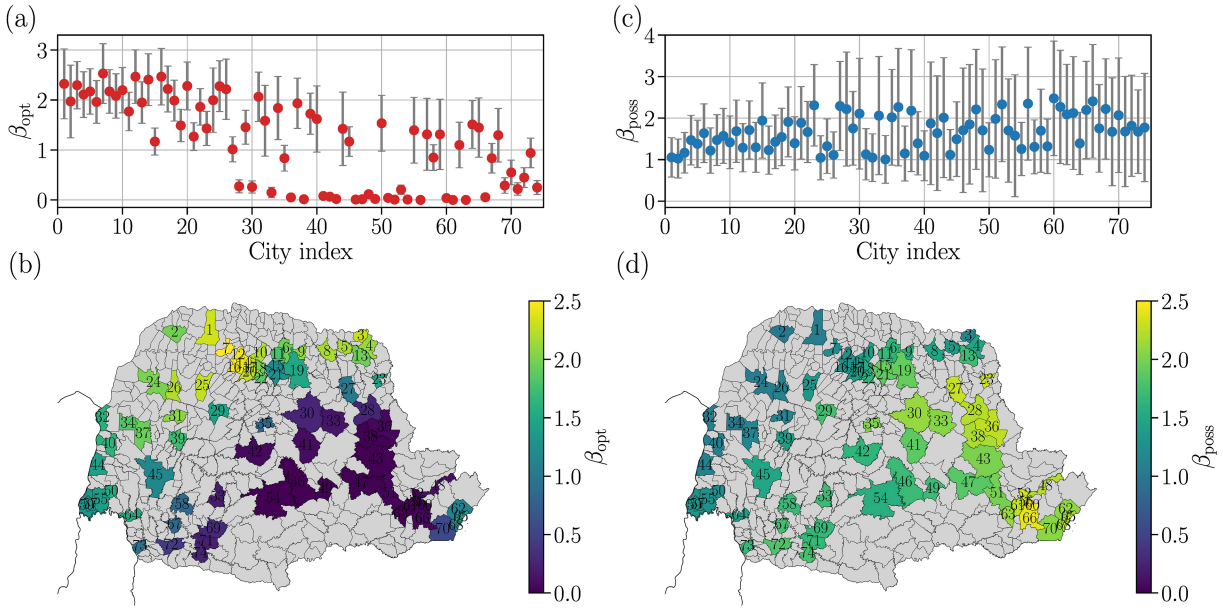


Figure 5. Regression coefficients from equation (5.1) for (a,b) optimal and (c,d) possible thermal days. The regression quantifies the effect of temperature anomaly on the monthly number of thermally permissive days. Panels (a) and (c) show the coefficients as a function of city index, with error bars representing 95% confidence intervals. Panels (b) and (d) show the corresponding spatial distributions.

days, especially in southern cities, which are historically cooler regions. Furthermore, figure 5*d* shows a cluster of municipalities with $\beta_{poss} > 1.2$ that coincides with the municipalities most affected in figure 3*c*. Thus, in cooler cities, anomalous warming does not always expand the number of days within the optimal transmission range, but it does increase the number of thermally possible days.

The regression coefficients are statistically significant, with a mean $p = 0.01$ for optimal days (63 cities with $p < 0.05$) and 0.003 for possible days (all 74 cities with $p < 0.05$). These results reinforce that temperature anomalies are associated with increases in both optimal and possible thermal days. Previous results established a robust relationship between temperature anomalies and thermally conducive days. We now assess whether these thermal conditions are associated with spatio-temporal synchronization.

As is well known, climate effects translate into dengue transmission with a delay. To estimate the time lag between thermally favourable days and synchronization, we conducted a cross-correlation analysis by progressively shifting one time series relative to

Downloaded from royalsocietypublishing.org/rsif/article-pdf/doi/10.1098/rsif.2026.0438/6159915/rsif.2026.0438.pdf
by guest
on 05 November 2026

Table 1. Estimated regression coefficients (β_1) for the association between thermal suitability indicators and synchronization. Results are shown for the linear model, the logistic component of the hurdle model for asynchronous states and the gamma component for positive synchronization values. Predictors correspond to the number of optimal (opt.) and possible (poss.) thermal days.

model	y	β_1 [95% CI]	p	R^2
linear	opt.	0.019 [0.013, 0.025]	6.8×10^{-10}	0.200
	poss.	0.004 [0.002, 0.006]	1.7×10^{-6}	0.122
	opt. + poss.	0.017 [0.011, 0.023], 0.003 [0.001, 0.005]	8.7×10^{-8}, 2.5×10^{-4}	0.256
logit	opt.	−0.396 [−0.622, −0.170]	5.7×10^{-4}	—
	poss.	−0.100 [−0.140, −0.056]	5.5×10^{-6}	—
	opt. + poss.	−0.311 [−0.529, −0.094], −0.080 [−0.123, −0.036]	5.0×10^{-3}, 3.0×10^{-4}	—
gamma	opt.	0.106 [0.032, 0.180]	4.9×10^{-3}	
	poss.	0.082 [0.052, 0.112]	6.0×10^{-8}	—
	opt. + poss.	0.084 [0.019, 0.150], 0.072 [0.042, 0.103]	1.1×10^{-2}, 3.5×10^{-6}	—

the other and calculating the correlation at each lag. The optimal lag was defined as that corresponding to the maximum correlation coefficient. The same procedure was repeated for the rainy variables. Mean monthly synchronization was most strongly associated with the number of optimal days at a lag of three months ($r = 0.44$). For possible days, the maximum correlation was achieved with a one-month delay ($r = 0.34$). Both delays are consistent with the literature [25].

To quantify the contribution of thermal suitability to synchronization, we evaluated three regression models. First, we considered a linear model, given by

$$\mathrm{Syn}(t) = \beta_0 + \beta_1 y(t - \ell) + \epsilon(t), \tag{5.2}$$

where $y(t - \ell)$ denotes the climate predictor lagged by ℓ. In this case, y represents thermal permissibility. This model captures linear associations between synchronization and thermal indicators.

Since $\mathrm{Syn}(t)$ contains a large proportion of zero values (approx. 46%), we used a hurdle model consisting of a logistic component for $\mathrm{Syn}(t) = 0$, defined by

$$P(\mathrm{Syn}(t) = 0 \mid y(t - \ell)) = \frac{1}{1 + e^{-(\beta_0 + \beta_1 y(t-\ell))}}, \tag{5.3}$$

and a gamma generalized linear model with log link for $\mathrm{Syn}(t) > 0$, given by

$$\mathbb{E}\left[\mathrm{Syn}(t) \mid \mathrm{Syn}(t) > 0, y(t - \ell)\right] = \exp\left(\beta_0^{(G)} + \beta_1^{(G)} y(t - \ell)\right). \tag{5.4}$$

For the three models, the regression results are summarized in table 1. The linear model reveals positive and statistically significant values of β_1, suggesting a positive association between thermal indicators and synchronization. Comparing both indicators, the number of optimal days has a stronger association with synchronization than the number of possible days. When both variables are included in a multiple regression, the linear model achieves $R^2 = 0.256$, higher than the simple-regression models. This suggests that combining both variables improves model fit, while preserving the stronger contribution of optimal days.

We then examined the nonlinear components of the hurdle model. The logistic component shows consistently negative values of β_1 with statistical significance for all three model specifications: optimal days, possible days and the multiple regression model. Again, optimal days show a stronger association than possible thermal days. These results indicate that increases in the number of thermally favourable days per month are associated with a reduced probability of observing asynchronous states. Therefore, conducive thermal conditions, with appropriate delays, are associated with the emergence of synchronization, with a dominant contribution from optimal days.

For observations with $\mathrm{Syn}(t) > 0$, the gamma model was employed. The results listed in table 1 show positive and statistically significant parameters, suggesting a nonlinear association between thermal permissibility and the magnitude of synchronization. These results indicate that, once synchronization is present, thermally favourable days, with appropriate delays, are associated with higher synchronization levels. Again, optimal days show a stronger association than possible days.

Taken together, our findings support a two-stage mechanism linking temperature anomalies to dengue synchronization: (i) anomalous warming increases the number of thermally permissive days and is associated with a reduced probability of asynchronous states, and (ii) once synchronization is present, appropriate thermal conditions are associated with higher synchronization levels. These results suggest that temperature may play a dual role in dengue synchronization, first favouring its emergence and subsequently sustaining the synchronous regime.

Downloaded from royalsocietypublishing.org/rsif/article-pdf/doi/10.1098/rsif.2026.0438/6159915/rsif.2026.0438.pdf
by guest
on 05 November 2026

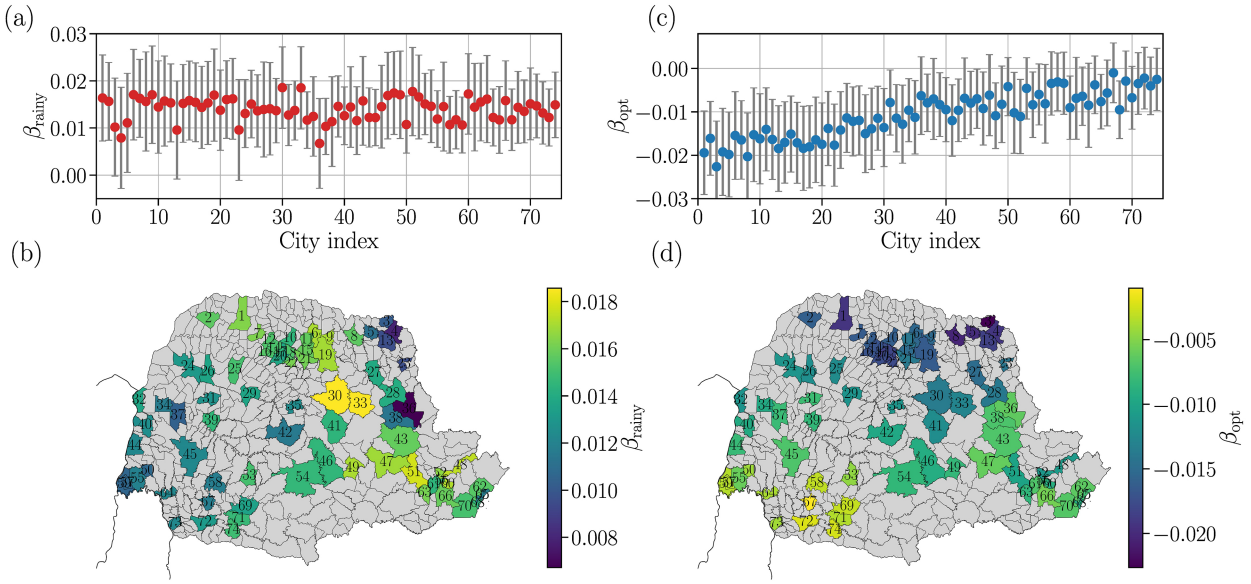


Figure 6. Regression coefficients from equation (5.1) for (a and b) rainy and (c and d) optimal precipitation days. The regression quantifies the effect of precipitation anomaly on the monthly number of precipitation-defined days. Panels (a) and (c) show the coefficients as a function of city index, with error bars representing 95% confidence intervals. Panels (b) and (d) show the corresponding spatial distributions.

Table 2. Classification of precipitation regimes according to quantiles and correlation between the number of days within each classification and precipitation anomalies (an.).

classification	quantile (Q)	correlation (an.)
very dry	$y \leq 0.15Q$	−0.285
dry	$0.15Q < y \leq 0.35Q$	−0.370
optimal/normal	$0.35Q < y \leq 0.65Q$	−0.180
rainy	$0.65Q \leq y < 0.85Q$	0.251
very rainy	$y \geq 0.85Q$	0.755

5.2. Anomalous precipitation and synchronization

Precipitation is also an important factor in dengue transmission. To assess its effects, we classified rainy days according to the quantile technique [79], as listed in table 2. By computing the correlation between the number of days within each classification and precipitation anomaly, we found a high correlation between precipitation anomaly and very rainy days. A weak positive correlation was observed for rainy days, while weak to moderate negative correlations were found for the other categories. These results indicate that precipitation anomalies do not lead to a uniform increase in rainfall, but are instead associated with changes in rainfall patterns, mainly characterized by more frequent very rainy days.

The observed changes of rainfall patterns are further supported by linear regression analyses (equation (5.2)), which yield positive coefficients for rainy days per month in all cities (figure 6*a*,*b*). Although the magnitude of β_{rainy} remains relatively small (approx. 0.01), a small increase in the number of rainy days as a function of precipitation anomaly is evident. By contrast, the linear regression performed for optimal precipitation days shows negative coefficients across the cities (figure 6*c*,*d*). Moreover, β_{opt} exhibits a spatial organization, increasing approximately linearly as a function of city index, suggesting that northern municipalities have fewer optimal precipitation days under positive anomalies. In southern municipalities, the number of optimal precipitation days remains practically unchanged.

The effects of precipitation on dengue synchronization are also expected to occur with a delay. Cross-correlation analysis shows that the strongest association between optimal precipitation days and synchronization occurs at a lag of four months ($r = 0.210$), whereas rainy days show a stronger association at a lag of two months ($r = 0.395$). These results suggest that optimal precipitation days are associated with synchronization at a longer lag and with a weaker correlation than rainy days.

Similar to the temperature analysis, we performed regressions between precipitation variables and synchronization; a summary of the results is listed in table 3. For the linear models, both variables yield positive and statistically significant coefficients ($p < 0.05$). The strongest association is observed for rainy days, which present a larger coefficient and a lower p-value than optimal

Downloaded from royalsocietypublishing.org/rsif/article-pdf/doi/10.1098/rsif.2026.0438/6159915/rsif.2026.0438.pdf
by guest
on 05 November 2026

Table 3. Estimated regression coefficients (β_1) obtained from the linear model (equation (5.2)) and from the two components of the hurdle model: the logistic regression for $P(\text{Syn} = 0)$ (equation (5.3)) and the gamma generalized linear model with log link for $\mathbb{E}[\text{Syn} \mid \text{Syn} > 0]$ (equation (5.4)). Predictors correspond to the number of optimal (opt.) and rainy precipitation days per month, while the response variable is the synchronization index.

model	*y*	β_1 [95% CI]	*p*	R^2
linear	opt.	0.006 [0.002, 0.010]	5.0×10^{-3}	0.045
	rainy	0.011 [0.007, 0.015]	4.4×10^{-8}	0.160
	opt. + rainy	0.005 [0.001, 0.008], 0.011 [0.007, 0.015]	2.0×10^{-2}, 3.0×10^{-7}	0.180
logit	opt.	−0.027 [−0.103, 0.048]	4.7×10^{-1}	–
	rainy	−0.220 [−0.318, −0.121]	1.1×10^{-5}	–
	opt. + rainy	−0.005 [−0.085, 0.074], −0.214 [−0.314, −0.115]	8.9×10^{-1}, 2.4×10^{-5}	–
gamma	opt.	0.091 [0.034, 0.149]	1.6×10^{-3}	–
	rainy	0.075 [0.021, 0.130]	6.6×10^{-3}	–
	opt. + rainy	0.080 [0.024, 0.133], 0.118 [0.061, 0.174]	4.4×10^{-3}, 3.8×10^{-5}	–

precipitation days. This difference becomes more evident when both variables are included simultaneously in a multiple regression model.

We then performed the hurdle model analysis. In the logit component, the estimated coefficients for rainy days are negative and statistically significant, indicating that wet conditions are associated with a reduced probability of asynchronous states. In this analysis, rainy days emerge as the dominant variable, with a coefficient approximately eight times greater in magnitude than the coefficient associated with optimal precipitation days. This difference is also observed in the multiple regression model.

For observations with non-null synchronization, we used the gamma model. When optimal and rainy variables are considered separately, both show positive coefficients, with a larger coefficient associated with optimal precipitation days. In the multiple regression model, however, rainy days become dominant, although the difference between coefficients is substantially reduced. This finding suggests that while rainy days are more strongly associated with the emergence of synchronization, both precipitation variables contribute to maintaining higher synchronization levels.

5.3. Multiple regression model—temperature and precipitation

The previous results suggest that temperature and precipitation are associated with a two-stage mechanism in synchronization, whereby they are linked to a reduced likelihood of asynchronous states and, subsequently, to the maintenance of coherent activity across the network. We now consider regression models including all four climatic variables, exemplified by

$$\begin{aligned}\text{Syn}(t) = \beta_0 &+ \beta_1 \,\text{opt. temp.}(t - \ell_1) + \beta_2 \,\text{poss. temp.}(t - \ell_2) \\ &+ \beta_3 \,\text{opt. prec.}(t - \ell_3) + \beta_4 \,\text{rainy}(t - \ell_4) + \epsilon(t),\end{aligned} \tag{5.5}$$

where β_1 and β_2 are associated with optimal and possible temperature, respectively, while β_3 and β_4 correspond to optimal precipitation and rainy days, respectively. The time lags for each variable were determined beforehand using cross-correlation analysis.

To remain consistent with the previous analyses, we estimate the associated parameters using linear, logistic and gamma models, with the results listed in table 4. Overall, the multiple regression framework provides a more comprehensive description of the observed synchronization patterns.

All models capture distinct contributions of each variable, with the strongest associations observed for the number of rainy days and optimal temperature. The former is related to the availability of breeding sites for mosquito populations, while the latter reflects favourable thermal conditions for mosquito development and virus transmission [80–82].

The logistic component shows negative and statistically significant coefficients for most variables, indicating that increases in the number of climatically favourable days are associated with a reduced probability of asynchronous states. This result is consistent with previous findings.

For observations with $\text{Syn}(t) > 0$, the gamma model shows positive and statistically significant coefficients, suggesting that climatic conditions are associated with higher levels of synchronization once present.

Taken together, these results are consistent with a two-stage mechanism in which climatic conditions are associated with both the emergence and persistence of synchronization. These findings highlight the role of climate variability in shaping the collective dynamics of dengue outbreaks. In addition, it is important to note that such favourable climatic conditions may become more frequent under climate change, particularly in temperate regions.

Downloaded from royalsocietypublishing.org/rsif/article-pdf/doi/10.1098/rsif.2026.0438/6159915/rsif.2026.0438.pdf
by guest
on 05 November 2026

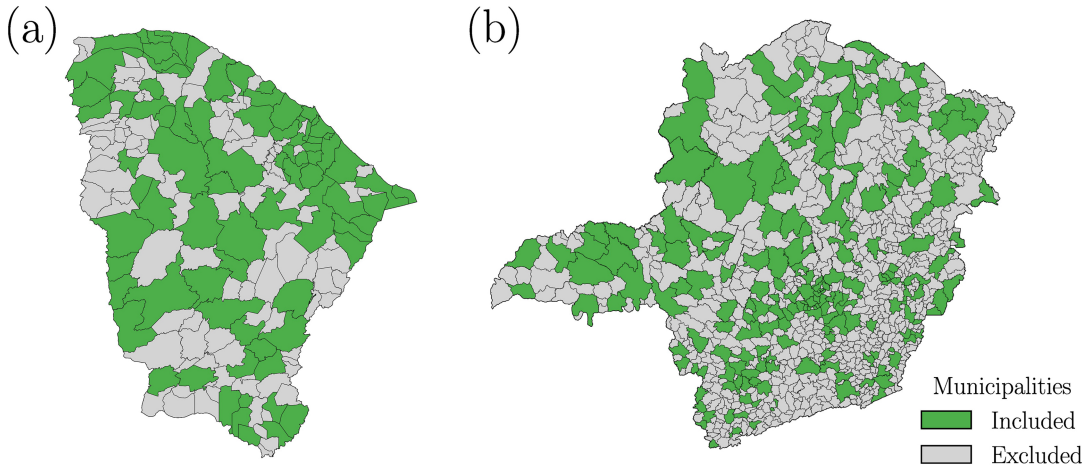


Figure 7. Included (green) and excluded (grey) municipalities in the cross-validation analysis for Ceará (panel (a)) and Minas Gerais (panel (b)). The inclusion criteria were: (i) municipalities with more than 20 000 inhabitants and (ii) municipalities reporting more than 1000 cumulative dengue cases during the study period (2010–2024). The maps are shown at different scales; therefore, the apparent sizes of Ceará and Minas Gerais are not representative of their actual relative areas.

Table 4. Multi-variate climate–synchronization regression results. Estimates are reported as β [95% CI] with corresponding p for the linear model, the logistic component (probability of an asynchronous state) and the gamma component (magnitude of synchronization conditional on Syn > 0). The parameters β_1, β_2, β_3 and β_4 are associated with optimal temperature (lag of three months), possible temperature (lag of one month), optimal precipitation (lag of four months) and rainy days (lag of two months), respectively. For the linear model, we obtain $R^2 = 0.328$.

	linear		logit		gamma	
	β [95% CI]	p	β [95% CI]	p	β [95% CI]	p
β_1	0.014 [0.008, 0.020]	8.09×10^{-6}	−0.300 [−0.528, −0.071]	1.0×10^{-2}	0.064 [0.000, 0.128]	4.8×10^{-2}
β_2	0.003 [0.001, 0.005]	5.4×10^{-3}	−0.057 [−0.105, −0.010]	1.8×10^{-2}	0.051 [0.018, 0.083]	2.0×10^{-3}
β_3	0.004 [0.001, 0.008]	2.2×10^{-2}	−0.011 [−0.104, 0.082]	8.1×10^{-1}	0.057 [0.005, 0.109]	3.0×10^{-2}
β_4	0.006 [0.002, 0.011]	2.6×10^{-3}	−0.134 [−0.241, −0.026]	1.5×10^{-2}	0.076 [0.018, 0.134]	9.7×10^{-3}

6. Validation in different localities

To explore the generality and limitations of the two-stage mechanism, we repeated the analysis for two additional Brazilian states: Ceará (figure 7*a*) and Minas Gerais (figure 7*b*). As inclusion criteria for municipalities, we used the same criteria as those applied to Paraná. Therefore, municipalities marked in green in figure 7 were included in the analysis, while those shown in grey were excluded.

First, we estimated the climatic lags for the 81 selected municipalities out of 184 in Ceará using cross-correlation analysis. Optimal temperature exhibited a maximum correlation of 0.52 with synchronization at a lag of six months, whereas possible temperature reached a weaker maximum correlation of 0.19 at eight months. For precipitation variables, optimal precipitation showed a moderate correlation of 0.265 at a lag of four months, while the number of rainy days displayed a substantially stronger correlation of 0.650 at a lag of 14 months. These lag structures suggest distinct temporal pathways linking climatic exposure to epidemic coherence. While thermal suitability appears to be associated with synchronization on intermediate time scales (six to eight months), rainfall, particularly rainy days, operates over longer temporal windows, potentially reflecting cumulative ecological effects on vector population dynamics. In addition, the relatively long lags identified for some climatic variables are not interpreted as direct causal delays between climate and dengue synchronization. Instead, in these cases, the lags reflect the persistence and seasonality of climatic conditions, as well as longer-term epidemiological characteristics. These climatic conditions can influence vector abundance across multiple transmission seasons, leading to long statistical associations.

We then incorporated these lags into the multi-variate regression framework (table 5). In the linear model, optimal temperature (β_1), optimal precipitation (β_3) and rainy days (β_4) are positively and significantly associated with synchronization, with rainy days showing the strongest association ($p < 10^{-12}$). By contrast, possible temperature (β_2) does not exhibit a significant linear contribution.

Downloaded from royalsocietypublishing.org/rsif/article-pdf/doi/10.1098/rsif.2026.0438/6159915/rsif.2026.0438.pdf
by guest
on 05 November 2026

Table 5. Multi-variate climate–synchronization regression results for Ceará. Estimates are reported as β [95% CI] with corresponding p for the linear model, the logistic component (probability of an asynchronous state), and the gamma component (magnitude of synchronization conditional on Syn > 0). The parameters β_1, β_2, β_3 and β_4 are associated with optimal temperature (lag of six months), possible temperature (lag of eight months), optimal precipitation (lag of four months) and rainy days (lag of 14 months), respectively.

	Ceará					
	linear		logit		gamma	
	β [95% CI]	p	β [95% CI]	p	β [95% CI]	p
β_1	0.003 [0.001, 0.004]	4.0×10^{-4}	0.014 [−0.078, 0.107]	7.5×10^{-1}	0.032 [0.020, 0.043]	7.3×10^{-8}
β_2	0.005 [−0.011, 0.020]	5.4×10^{-1}	−0.616 [−1.695, 0.463]	2.6×10^{-1}	0.077 [−0.049, 0.203]	2.3×10^{-1}
β_3	0.003 [0.001, 0.005]	7.0×10^{-4}	−0.163 [−0.394, 0.069]	1.6×10^{-1}	0.013 [−0.003, 0.029]	1.1×10^{-1}
β_4	0.010 [0.007, 0.012]	1.12×10^{-12}	−0.688 [−1.605, 0.229]	1.4×10^{-1}	0.075 [0.055, 0.095]	1.5×10^{-13}

The logistic component does not reveal statistically significant predictors, indicating that in Ceará, the climate variables are not strongly associated with the probability of asynchronous states. This contrasts with more transitional settings, where climatic permissibility appears to be associated with the emergence of coherent epidemic activity, and suggests that baseline climatically conducive days in Ceará may already sustain persistent epidemic coherence.

The gamma regression reveals a different pattern. Conditional on synchronization being present (Syn > 0), both optimal temperature and rainy days are significantly associated with a higher magnitude of synchronization, with highly robust effects ($p < 10^{-7}$ and $p < 10^{-13}$, respectively). This indicates that, although climate does not appear to be associated with the onset of synchronization in Ceará, it is strongly associated with its intensity.

Taken together, these results point to a regime characterized by persistent baseline synchronization, where climatic variability appears to act primarily as an amplifier rather than as a trigger. This behaviour is consistent with the semi-arid tropical climate of Ceará, where thermal suitability is maintained for most of the year and rainfall pulses may generate delayed and cumulative effects on vector abundance.

Compared with Ceará, the 180 selected municipalities from Minas Gerais exhibit a different structure in the climate–synchronization relationship (table 6). In the linear component, all predictors are positively and significantly associated with synchronization, indicating that both thermal and precipitation suitability are associated with coherent epidemic dynamics across cities. In particular, optimal temperature (β_1) and rainy days (β_4) display the strongest associations, suggesting that favourable thermal conditions and rainfall are linked to spatial epidemic coherence. For this model, we obtained $R^2 = 0.38$.

The main difference compared with Ceará appears in the logistic component. In Minas Gerais, both possible temperature (β_2) and rainy days (β_4) are statistically significant and negative. This indicates that climatic permissibility is associated with a reduced likelihood of asynchronous epidemic activity. In this sense, adequately lagged meteorological conditions are associated with increased coherence among outbreaks across the state. This result is similar to that observed in Paraná, where the components β_1, β_2 and β_4 are associated with a reduced probability of asynchronous states.

Once synchronization is present, the gamma regression results in table 6 indicate that most climatic variables are associated with higher synchronization levels, except β_1, whose confidence interval crosses zero. These results suggest that climate in Minas Gerais is associated not only with the emergence of synchronized states, but also with the maintenance of spatial coherence.

7. Sensitivity analysis of the synchronization window and outbreak threshold

We performed a sensitivity analysis to quantify how the synchronization window (τ) and outbreak threshold affect the average synchronization over the entire time series, denoted by $\overline{\text{Syn}}$.

In the main analysis, outbreaks were defined using the condition $c_i(t) \geq \bar{c}_i + 1$. To explore a broader range of outbreak definitions, we generalized this threshold to $c_i(t) \geq \bar{c}_i + 1 + k\,\sigma_i$, where σ_i is the standard deviation of each municipal time series and k is a constant.

As a reference, we considered the average synchronization obtained for $\tau = 2$ and $k = 0$. The relative impact of each parameter combination was then defined as

$$\text{impact}(\tau, k) = \left(\overline{\text{Syn}}(\tau, k) - \overline{\text{Syn}}(2, 0)\right) \times 100\%. \tag{7.1}$$

First, fixing $k = 0$, we evaluated the effect of varying τ. The results, shown in figure 8*a*, indicate that for $\tau = 1$, the average synchronization decreases, whereas for $\tau > 2$, it increases monotonically. For all three states, Paraná (PR), Minas Gerais (MG) and Ceará (CE), the impact grows approximately linearly with τ. This behaviour is expected, as the synchronization measure is defined through a temporal window that accumulates coincident events, leading to an inherent dependence on τ.

Downloaded from royalsocietypublishing.org/rsif/article-pdf/doi/10.1098/rsif.2026.0438/6159915/rsif.2026.0438.pdf
by guest
on 05 November 2026

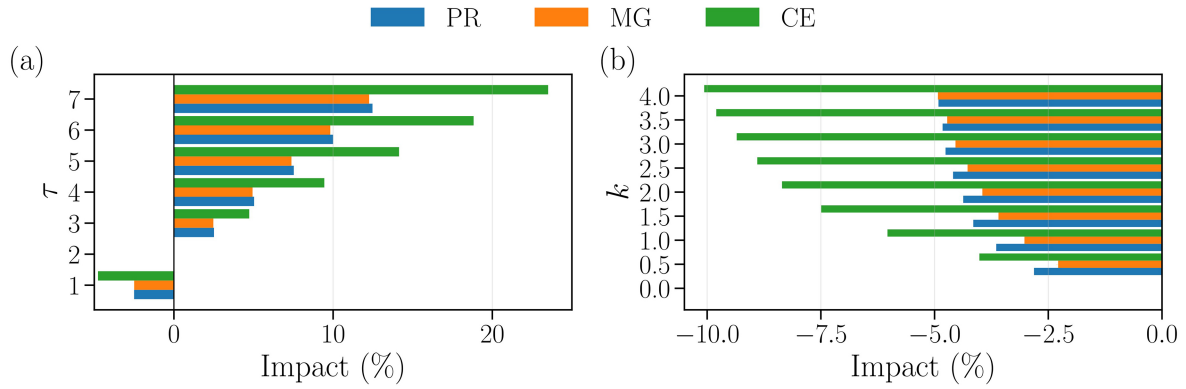


Figure 8. Sensitivity analysis of the average synchronization $\overline{\text{Syn}}$ with respect to the synchronization window τ and the outbreak threshold parameter k. The impact is defined relative to the baseline case ($\tau = 2$ and $k = 0$) as $\text{impact}(\tau, k) = \left(\overline{\text{Syn}}(\tau, k) - \overline{\text{Syn}}(2, 0)\right) \times 100\%$. (a) Impact of varying the synchronization window τ while fixing $k = 0$. (b) Impact of varying the threshold parameter k while fixing $\tau = 2$. Results are shown for Paraná (PR), Minas Gerais (MG) and Ceará (CE) in blue, orange and green, respectively.

Table 6. Multi-variate climate–synchronization regression results for Minas Gerais. Estimates are reported as β [95% CI] with corresponding p for the linear model, the logistic component (probability of an asynchronous state) and the gamma component (magnitude of synchronization conditional on Syn > 0). The parameters β_1, β_2, β_3 and β_4 are associated with optimal temperature (lag of four months), possible temperature (lag of four months), optimal precipitation (lag of 12 months) and rainy days (lag of one month), respectively.

	Minas Gerais					
	linear		logit		gamma	
	β [95% CI]	p	β [95% CI]	p	β [95% CI]	p
	β [95% CI]	p	β [95% CI]	p	β [95% CI]	p
β_1	0.014 [0.007, 0.021]	8.0×10^{-5}	−0.813 [−2.320, 0.694]	2.9×10^{-1}	0.088 [−0.003, 0.179]	5.7×10^{-2}
β_2	0.005 [0.002, 0.008]	1.8×10^{-3}	−0.215 [−0.328, −0.103]	1.6×10^{-4}	0.111 [0.037, 0.185]	3.3×10^{-3}
β_3	0.004 [0.001, 0.007]	1.3×10^{-2}	−0.005 [−0.111, 0.101]	9.2×10^{-1}	0.058 [0.012, 0.103]	1.3×10^{-2}
β_4	0.008 [0.005, 0.011]	4.9×10^{-8}	−0.279 [−0.396, −0.161]	3.2×10^{-6}	0.113 [0.069, 0.157]	5.7×10^{-7}

Next, fixing $\tau = 2$, we analysed the effect of varying the threshold parameter k, as shown in figure 8*b*. In this case, the dependence is nonlinear and exhibits a systematic decrease in synchronization as k increases. This reflects the progressive filtering of weaker outbreaks, which reduces the number of detected events and, consequently, the likelihood of temporal coincidence across cities.

Importantly, despite these quantitative changes, the qualitative patterns remain consistent across parameter values. In particular, Ceará exhibits stronger sensitivity to both τ and k, while Paraná and Minas Gerais display similar responses. These results indicate that our main findings are robust with respect to the choice of synchronization window and outbreak definition.

8. Conclusions

In this study, we systematically analysed the long-term transmission of dengue fever across 74 municipalities in Paraná, Brazil, between 2010 and 2024. Historically, this subtropical state exhibited relatively low dengue incidence compared with other Brazilian states, with cases spatially restricted to a limited subset of cities. Our analyses reveal a clear epidemiological transition after 2020, marking a shift characterized by the expansion of dengue into previously less-affected municipalities.

The post-break point regime is characterized by a pronounced geographic expansion of dengue and by a substantial change in the spatio-temporal pattern of outbreaks. Dengue transmission becomes increasingly synchronized across cities, reflecting a transition from localized, seasonally constrained epidemics to a more coherent dynamical state. Although high synchronization typically coincides with large outbreaks, the unprecedented epidemic of 2024 exhibits a distinct pattern: synchronization is sustained over long periods through multiple overlapping waves, rather than being dominated by a single seasonal peak. This shift is accompanied by a substantial change in the dengue season, with outbreaks emerging earlier, persisting longer and occurring even during winter months.

Downloaded from royalsocietypublishing.org/rsif/article-pdf/doi/10.1098/rsif.2026.0438/6159915/rsif.2026.0438.pdf
by guest
on 05 November 2026

To investigate potential drivers of this transition, we examined the role of climatic forcing, focusing on temperature and precipitation anomalies. We show that anomalous weather conditions are associated with a substantial increase in the number of thermally and hydrologically conducive days for dengue transmission. Importantly, these increases are not uniform but reflect a reshaping of climatic conditions, with warming and intensified rainfall extremes.

Our results support a two-stage mechanism linking climate anomalies to dengue synchronization. First, the expansion of climate-conducive days is associated with a reduced probability of asynchronous states and with the emergence of coherent transmission across cities. Once synchronization is established, climatic suitability is further associated with higher and more persistent synchronization through delayed nonlinear effects. This mechanism provides a useful framework for connecting climate variability, geographical expansion and large-scale epidemic coherence.

Taken together, our findings suggest that changing climatic conditions may be reshaping the dynamics of dengue in Paraná, contributing to the transformation of a spatially fragmented and seasonal disease into a more persistent and regionally synchronized public health threat. Beyond its regional relevance, this study highlights how gradual climatic changes may contribute to abrupt epidemiological transitions by altering the collective dynamics of disease spread.

To assess the robustness of our findings across different climatic regimes, we extended the analysis to two additional Brazilian states, Ceará and Minas Gerais. Comparing the results for the three states, we find a consistent pattern in the linear component, with statistically significant associations for most predictors across all regions. However, the proposed two-stage mechanism is not universally expressed. The logistic regression indicates that conducive climatic conditions are significantly associated with a reduced probability of asynchronous epidemic states in Paraná and Minas Gerais, whereas this effect is not observed in Ceará. We argue that this difference may be associated with the persistent climatic suitability in Ceará, where temperatures remain within the optimal or possible range for mosquito development during most of the year. Under such conditions, synchronization may not require an additional climatic trigger. By contrast, the gamma component, which captures the magnitude and maintenance of synchronization once it is established, is statistically significant in all three states. This suggests that favourable climatic conditions consistently enhance the temporal persistence and spatial coherence of dengue outbreaks, even though their role in the emergence of synchronization may depend on the regional climatic context. Our results highlight the important role of climate conditions in shaping dengue synchronization, acting through a two-stage mechanism: first, favouring the emergence of synchronous regimes and subsequently sustaining them. These findings underscore the need to incorporate climate-sensitive synchronization indicators into dengue surveillance, early-warning systems and adaptation strategies, particularly in temperate and subtropical regions that are becoming increasingly vulnerable under ongoing climate change.

Ethics. This work did not require ethical approval from a human subject or animal welfare committee.

Data accessibility. The data and code are fully available on [83].

Declaration of AI use. The authors used generative artificial intelligence tools to assist with language editing during manuscript preparation.

Authors' contributions. E.C.G.: conceptualization, data curation, formal analysis, investigation, methodology, project administration, software, validation, visualization, writing—original draft, writing—review and editing; A.M.B.: funding acquisition, resources, supervision, writing—original draft, writing—review and editing; I.C.: conceptualization, funding acquisition, methodology, project administration, resources, supervision, writing—review and editing; J.K.: conceptualization, methodology, supervision, writing—review and editing; M.A.: conceptualization, methodology, supervision, validation, visualization, writing—original draft, writing—review and editing.

All authors gave final approval for publication and agreed to be held accountable for the work performed therein.

Conflict of interest declaration. We declare we have no competing interests.

Funding. I.C. is funded by CNPq (grant no. 302665/2017-0), Coordenação de Aperfeiçoamento de Pessoal de Nível Superior (CAPES) and FAPESP (grant no. 2024/05700-5). E.C.G. acknowledges financial support from FAPESP under grants nos. 2025/02318-5 and 2025/24097-0. A.M.B. acknowledges financial support from CNPq, CAPES and FAPESP (grant no. 2025/14690-6). M.A. acknowledges financial support from the Spanish Ministerio de Ciencia e Innovación (MICINN) through the Ramón y Cajal grant RYC2021-031380-I. This research was supported by the Basque Government through the 'Mathematical Modeling Applied to Health' project (BERC 2022–2025 programme) and by the Spanish Ministry of Science, Innovation and Universities through the BCAM Severo Ochoa accreditation CEX2021-001142-S (MICINN/AEI/10.13039/501100011033).

References

1. Organization WH. 2025 *Dengue*. https://www.who.int/news-room/fact-sheets/detail/dengue-and-severe-dengue.
2. Bhatt S *et al.* 2013 The global distribution and burden of dengue. *Nature* **496**, 504–507. (doi:10.1038/nature12060)
3. Simmons CP, Farrar JJ, van Vinh Chau N, Wills B. 2012 Dengue. *N. Engl. J. Med.* **366**, 1423–1432. (doi:10.1056/NEJMra1110265)
4. Kularatne SA, Dalugama C. 2022 Dengue infection: global importance, immunopathology and management. *Clin. Med.* **22**, 9–13. (doi:10.7861/clinmed.2021-0791)
5. Dash MK, Samal S, Rout S, Behera CK, Sahu MC, Das B. 2024 Immunomodulation in dengue: towards deciphering dengue severity markers. *Cell Commun. Signal.* **33**, 451. (doi:10.1186/s12964-024-01779-4)
6. Guzman MG, Harris E. 2015 Dengue. *Lancet* **385**, 453–65. (doi:10.1016/S0140-6736(14)60572-9)
7. Sebayang AA, Fahlena H, Anam V, Knopoff D, Stollenwerk N, Aguiar M, Soewono E. 2021 Modeling dengue immune responses mediated by antibodies: a qualitative study. *Biology* **10**, 941. (doi:10.3390/biology10090941)
8. Anam V, Guerrero BV, Srivastav AK, Stollenwerk N, Aguiar M. 2024 Within-host models unravelling the dynamics of dengue reinfections. *Infect. Dis. Model.* **9**, 458–473. (doi:10.1016/j.idm.2024.02.004)
9. Aguiar M, Ballesteros S, Stollenwerk N. 2010 Two strain dengue model with temporary cross immunity and seasonality. *AIP Conf. Proc.* **1281**, 732–735. (doi:10.1063/1.3498585)

Downloaded from royalsocietypublishing.org/rsif/article-pdf/doi/10.1098/rsif.2026.0438/6159915/rsif.2026.0438.pdf
by guest
on 05 November 2026

10. Aguiar M, Kooi BW, Martins J, Stollenwerk N. 2012 Scaling of stochasticity in dengue hemorrhagic fever epidemics. *Math. Model. Nat. Phenom.* **7**, 1–11. (doi:10.1051/mmnp/20127301)
11. Aguiar M, Kooi BW, Rocha F, Ghaffari P, Stollenwerk N. 2013 How much complexity is needed to describe the fluctuations observed in dengue hemorrhagic fever incidence data? *Ecol. Complex.* **16**, 31–40. (doi:10.1016/j.ecocom.2012.09.001)
12. Aguiar M, Paul R, Sakuntabhai A, Stollenwerk N. 2014 Are we modelling the correct dataset? Minimizing false predictions for dengue fever in Thailand. *Epidemiol. Infect.* **142,** 2447–2459. (doi:10.1017/S0950268813003348)
13. Steindorf V, Srivastav AK, Stollenwerk N, Kooi BW, Aguiar M. 2022 Modeling secondary infections with temporary immunity and disease enhancement factor: mechanisms for complex dynamics in simple epidemiological models. *Chaos Solit. Fractals* **164**, 112709. (doi:10.1016/j.chaos.2022.112709)
14. Aguiar M *et al*. 2022 Mathematical models for dengue fever epidemiology: a 10-year systematic review. *Phys. Life Rev.* **40**, 65–92. (doi:10.1016/j.plrev.2022.02.001)
15. Aguiar M, Stollenwerk N, Halstead SB. 2016 The impact of the newly licensed dengue vaccine in endemic countries. *PLoS Negl. Trop. Dis.* **10**, e0005179. (doi:10.1371/journal.pntd.0005179)
16. Aguiar M. 2018 Dengue vaccination: a more ethical approach is needed. *Lancet* **391**, 1769–1770. (doi:10.1016/s0140-6736(18)30865-1)
17. Aguiar M, Stollenwerk N. 2020 The impact of serotype cross-protection on vaccine trials: denvax as a case study. *Vaccines* **8**, 674. (doi:10.3390/vaccines8040674)
18. Srivastav AK, Steindorf V, Guerrero BV, Stollenwerk N, Kooi BW, Aguiar M. 2026 Bifurcation analysis of a two-infection transmission model with explicit vector dynamics. *J. Math. Biol.* **92**, 26. (doi:10.1007/s00285-026-02341-1)
19. Doutor P, Castelhano R, Soares MC, Guerrero BV, Stollenwerk N, Aguiar M. 2025 Complex dynamics in an epidemic model with imitation-driven vaccination strategy. *SIAM J. Appl. Dyn. Syst.* **24**, 3045–3062. (doi:10.1137/24m1703707)
20. Aguiar M, Ballesteros S, Kooi BW, Stollenwerk N. 2011 The role of seasonality and import in a minimalistic multi-strain dengue model capturing differences between primary and secondary infections: complex dynamics and its implications for data analysis. *J. Theor. Biol.* **289**, 181–196. (doi:10.1016/j.jtbi.2011.08.043)
21. Rocha F, Mateus L, Skwara U, Aguiar M, Stollenwerk N. 2014 Understanding dengue fever dynamics: a study of seasonality in vector-borne disease models. *Int. J. Comput. Math.* **93**, 1405–1422. (doi:10.1080/00207160.2015.1050961)
22. da Silva ST, Gabrick EC, Protachevicz PR, Iarosz KC, Caldas IL, Batista AM, Kurths J. 2025 When climate variables improve the dengue forecasting: a machine learning approach. *Eur. Phys. J. Spec. Top.* **234**, 555–569. (doi:10.1140/epjs/s11734-024-01201-7)
23. Merkenschlager C, Bangelesa F, Paeth H, Hertig E. 2025 Evolution of the recent habitat suitability area of *Aedes albopictus* in the extended Mediterranean area due to land-use and climate change. *Sci. Total Environ.* **974**, 179202. (doi:10.1016/j.scitotenv.2025.179202)
24. Gibb R *et al.* 2023 Interactions between climate change, urban infrastructure and mobility are driving dengue emergence in Vietnam. *Nat. Commun.* **14**, 8179. (doi:10.1038/s41467-023-43954-0)
25. Abdullah NAMH, Dom NC, Salleh SA, Salim H, Precha N. 2022 The association between dengue case and climate: a systematic review and meta-analysis. *One Health* **15**, 100452. (doi:10.1016/j.onehlt.2022.100452)
26. Mordecai EA *et al.* 2017 Detecting the impact of temperature on transmission of Zika, dengue, and chikungunya using mechanistic models. *PLoS Negl. Trop. Dis.* **11**, e0006935. (doi:10.1371/journal.pntd.0006424)
27. Lowe R *et al.* 2018 Nonlinear and delayed impacts of climate on dengue risk in Barbados: a modelling study. *PLoS Med.* **15**, e1002613. (doi:10.1371/journal.pmed.1002613)
28. Liu Y, Wang X, Tang B. 2025 A novel approach to quantify the optimal range and causal effect of rainfall on vector-borne diseases: a case study of dengue epidemics. *J. R. Soc. Interface* **22**, 20250029. (doi:10.1098/rsif.2025.0029)
29. Benedum CM, Seidahmed OME, Eltahir EAB, Markuzon N. 2018 Statistical modeling of the effect of rainfall flushing on dengue transmission in Singapore. *PLoS Negl. Trop. Dis.* **12**, e0006935. (doi:10.1371/journal.pntd.0006935)
30. Islam S, Haque CE, Hossain S, Rochon K. 2019 Role of container type, behavioural, and ecological factors in *Aedes* pupal production in Dhaka, Bangladesh: an application of zero-inflated negative binomial model. *Acta Trop.* **193**, 50–59. (doi:10.1016/j.actatropica.2019.02.019)
31. European Centre for Disease Prevention and Control. *World Mosquito Day 2025: Europe sets new records for mosquito-borne diseases*. https://www.ecdc.europa.eu/en/news-events/world-mosquito-day-2025-europe-sets-new-records-mosquito-borne-diseases.
32. European Centre for Disease Prevention and Control. *Seasonal surveillance of dengue in the EU/EEA*. https://www.ecdc.europa.eu/en/dengue/surveillance-and-updates/seasonal-surveillance-dengue-eueea-weekly.
33. de Souza WM, Weaver SC. 2024 Effects of climate change and human activities on vector-borne diseases. *Nat. Rev. Microbiol.* **22**, 476–491. (doi:10.1038/s41579-024-01026-0)
34. Nakase T, Giovanetti M, Obolski U, Lourenço J. 2024 Population at risk of dengue virus transmission has increased due to coupled climate factors and population growth. *Commun. Earth Environ.* **5**, 475. (doi:10.1038/s43247-024-01639-6)
35. Estallo EL, Sippy R, Robert MA, Ayala S, Pizard CJB, Pérez-Estigarribia PE, Stewart-Ibarra AM. 2023 Increasing arbovirus risk in Chile and neighboring countries in the Southern Cone of South America.*Lancet* **23**, 100542. (doi:10.1016/j.lansea.2025.100542)
36. Colón-González FJ, Sewe MO, Tompkins AM, Sjödin H, Casallas A, Rocklöv J, Caminade C, Lowe R. 2021 Projecting the risk of mosquito-borne diseases in a warmer and more populated world: a multi-model, multi-scenario intercomparison modelling study. *Lancet Planet Health* **5**, e404–e414. (doi:10.1016/s2542-5196(21)00132-7)
37. Stollenwerk N, Mateus L, Steindorf V, Guerrero BV, Blasco-Aguado R, Cevidanes A, Van-Dierdonck JB, Aguiar M. 2025 Evaluating the risk of mosquito-borne diseases in non-endemic regions: a dynamic modeling approach. *Math. Comput. Simul.* **238**, 1–24. (doi:10.1016/j.matcom.2025.04.026)
38. Guerrero BV *et al.* 2025 Assessing the spatio-temporal risk of *Aedes*-borne arboviral diseases in non-endemic regions: the case of Northern Spain. *PLoS Negl. Trop. Dis.* **19**, e0013325. (doi:10.1371/journal.pntd.0013325)
39. Pisaneschi G, Manfredi P, Landi A, Stollenwerk N, Aguiar M. 2026 When few mosquitoes are enough: dengue outbreaks in non-endemic areas. *One Health* **22**, 101308. (doi:10.1016/j.onehlt.2025.101308)
40. Steindorf V, B HMK, Stollenwerk N, Cevidanes A, Barandika JF, Vazquez P, García-Pérez AL, Aguiar M. 2025 Forecasting invasive mosquito abundance in the Basque Country, Spain using machine learning techniques. *Parasites Vectors* **18**, 109. (doi:10.1186/s13071-025-06733-y)
41. Baker RE *et al.* 2022 Infectious disease in an era of global change. *Nat. Rev. Microbiol.* **20**, 193–205. (doi:10.1038/s41579-021-00639-z)

Downloaded from royalsocietypublishing.org/rsif/article-pdf/doi/10.1098/rsif.2026.0438/6159915/rsif.2026.0438.pdf
by guest
on 05 November 2026

42. Metcalf CJE, Walter KS, Wesolowski A, Buckee CO, Shevliakova E, Tatem AJ, Boos WR, Weinberger DM, Pitzer VE. 2017 Identifying climate drivers of infectious disease dynamics: recent advances and challenges ahead. *Proc. R. Soc. B* **284**, 20170901. (doi:10.1098/rspb.2017.0901)
43. Charnley GEC *et al.* 2025 Strengthening resilience to emerging vector-borne diseases in Europe: lessons learnt from countries facing endemic transmission. *Lancet Reg. Health Eur.* **53**, 101271. (doi:10.1016/j.lanepe.2025.101271)
44. Tegar S, Brass DP, Purse BV, Cobbold CA, White SM. 2026 Temperature-sensitive incubation, transmissibility and risk of *Aedes albopictus*-borne chikungunya virus in Europe. *J. R. Soc. Interface* **23**, 20250707. (doi:10.1098/rsif.2025.0707)
45. Pereira SB, Bohm BC, dos Reis Gomes A, Gonçalves GA, Bruhn NCP, Belo VS, Aguilera-Benavente F, Bruhn FRP. 2025 Emergence and spatiotemporal incidence of dengue in Rio Grande do Sul, Brazil. *Sci. Rep.* **15**, 18933. (doi:10.1038/s41598-025-02548-0)
46. Ryan SJ, Carlson CJ, Mordecai EA, Johnson LR. 2019 Global expansion and redistribution of *Aedes*-borne virus transmission risk with climate change. *PLoS Negl. Trop. Dis.* **13**, e0007213. (doi:10.1371/journal.pntd.0007213)
47. Kraemer MUG *et al.* 2019 Past and future spread of the arbovirus vectors *Aedes aegypti* and *Aedes albopictus*. *Nat. Microbiol.* **4**, 854–863. (doi:10.1038/s41564-019-0376-y)
48. Barcellos C, Matos V, Lana RM, Lowe R. 2024 Climate change, thermal anomalies, and the recent progression of dengue in Brazil. *Sci. Rep.* **14**, 5948. (doi:10.1038/s41598-024-56044-y)
49. Finch E, Chang C-C, Kucharski A, Sim S, Ng L-C, Lowe R. 2025 Climate variation and serotype competition drive dengue outbreak dynamics in Singapore. *Nat. Commun.* **16,** 11364. (doi:10.1038/s41467-025-66411-6)
50. Childs ML, Lyberger K, Harris MJ, Burke M, Mordecai EA. 2025 Climate warming is expanding dengue burden in the Americas and Asia. *Proc. Natl Acad. Sci. USA* **122**, e2512350122. (doi:10.1073/pnas.2512350122)
51. Cox VM *et al*. 2025 Spatiotemporal relationships between extreme weather events and arbovirus transmission across Brazil. *eLife* **14**, RP108289. (doi:10.7554/eLife.108289.1)
52. Pikovsky A, Rosenblum M, Kurths J. 2001 *Synchronization: a universal concept in nonlinear sciences*. Cambridge, UK: Cambridge University Press.
53. Viboud C, Bjørnstad ON, Smith DL, Simonsen L, Miller MA, Grenfell BT. 2006 Synchrony, waves, and spatial hierarchies in the spread of influenza. *Science* **312**, 447–451. (doi:10.1126/science.1125237)
54. Quandelacy TM *et al.* 2025 Synchronized dynamics of dengue across the Americas. *Sci. Transl. Med.* **17**, eadq4326. (doi:10.1126/scitranslmed.adq4326)
55. van Panhuis WG *et al.* 2015 Region-wide synchrony and traveling waves of dengue across eight countries in Southeast Asia. *Proc. Natl Acad. Sci. USA* **112**, 13 069–13 074. (doi:10.1073/pnas.1501375112)
56. Garcia-Carreras B *et al*. 2022 Periodic synchronisation of dengue epidemics in Thailand over the last 5 decades driven by temperature and immunity. *PLoS Biol.* **20**, e3001160. (doi:10.1371/journal.pbio.3001160)
57. Schwartz IB, Shaw LB, Cummings DAT, Billings L, McCrary M, Burke DS. 2005 Chaotic desynchronization of multistrain diseases. *Phys. Rev. E* **72**, 066201. (doi:10.1103/PhysRevE.72.066201)
58. Churakov M, Villabona-Arenas CJ, Kraemer MUG, Salje H, Cauchemez S. 2019 Spatio-temporal dynamics of dengue in Brazil: seasonal travelling waves and determinants of regional synchrony. *PLoS Negl. Trop. Dis.* **13**, e0007012. (doi:10.1371/journal.pntd.0007012)
59. Rohani P, Earn DJD, Grenfell BT. 1999 Opposite patterns of synchrony in sympatric disease metapopulations. *Science* **286**, 968–971. (doi:10.1126/science.286.5441.968)
60. Earn DJD, Rohani P, Grenfell BT. 1998 Persistence, chaos and synchrony in ecology and epidemiology. *Proc. R. Soc. B* **265**, 7–10. (doi:10.1098/rspb.1998.0256)
61. Rodríguez JP, Eguíluz VM. 2023 Coupling between infectious diseases leads to synchronization of their dynamics. *Chaos* **33**, 021103. (doi:10.1063/5.0137380)
62. Cummings DAT, Irizarry RA, Huang NE, Endy TP, Nisalak A, Ungchusak K, Burke DS. 2004 Travelling waves in the occurrence of dengue haemorrhagic fever in Thailand. *Nature* **427**, 344–347. (doi:10.1038/nature02225)
63. Quiroga RQ, Kreuz T, Grassberger P. 2002 Event synchronization: a simple and fast method to measure synchronicity and time delay patterns. *Phys. Rev. E* **66**, 041904. (doi:10.1103/PhysRevE.66.041904)
64. Quiroga RQ, Kraskov A, Kreuz T, Grassberger P. 2002 Performance of different synchronization measures in real data: a case study on electroencephalographic signals. *Phys. Rev. E* **65**, 041903. (doi:10.1103/PhysRevE.65.041903)
65. Kreuz T, Haas JS, Morelli A, Abarbanel HDI, Politi A. 2007 Measuring spike train synchrony. *J. Neurosci. Methods* **165**, 151–161. (doi:10.1016/j.jneumeth.2007.05.031)
66. Pereda E, Quiroga RQ, Bhattacharya J. 2005 Nonlinear multivariate analysis of neurophysiological signals. *Prog. Neurobiol.* **77**, 1–37. (doi:10.1016/j.pneurobio.2005.10.003)
67. Tang Y, Luo M, Wu S, Li X. 2025 Increasing synchrony of extreme heat and precipitation events under climate warming. *Geophys. Res. Lett.* **52**, e2024GL113021. (doi:10.1029/2024gl113021)
68. Boers N, Goswami B, Rheinwalt A, Bookhagen B, Hoskins B, Kurths J. 2019 Complex networks reveal global pattern of extreme-rainfall teleconnections. *Nature* **566**, 373–377. (doi:10.1038/s41586-018-0872-x)
69. Su Z, Meyerhenke H, Kurths J. 2022 The climatic interdependence of extreme-rainfall events around the globe. *Chaos* **32**, 043126. (doi:10.1063/5.0077106)
70. Codeco C, Coelho F, Cruz O, Oliveira S, Castro T, Bastos L. 2018 Infodengue: a nowcasting system for the surveillance of arboviruses in Brazil. *Rev. Epidemiol. Santé Publique* **66**, S386. (doi:10.1016/j.respe.2018.05.408)
71. GOV P. *Boletins da dengue*. https://www.dengue.pr.gov.br/Pagina/Boletins-da-Dengue.
72. Instituto Brasileiro de Geografia e EstatÃstica. Censo Demográfico 2022. https://www.ibge.gov.br/estatisticas/sociais/saude/22827-censo-demografico-2.
73. Sabater JM. *ERA5-Land hourly data from 1950 to present.* Copernicus Climate Change Service (C3S) Climate Data Store (CDS). https://cds.climate.copernicus.eu/datasets/reanalysis-era5-land?tab=overview. (doi:10.24381/cds.e2161bac)
74. IBGE. *Malha municipal*. https://www.ibge.gov.br/geociencias/organizacao-do-territorio/malhas-territo%riais/.
75. Agarwal A, Marwan N, Rathinasamy M, Merz B, Kurths J. 2017 Multi-scale event synchronization analysis for unravelling climate processes: a wavelet-based approach. *Nonlin. Processes Geophys.* **24**, 599–611. (doi:10.5194/npg-24-599-2017)
76. Truong C, Oudre L, Vayatis N. 2020 Selective review of offline change point detection methods. *Signal Process.* **167**, 107299. (doi:10.1016/j.sigpro.2019.107299)
77. de Almeida MT, Merighi DGS, Visnardi AB, Gonçalves CAB, de Freitas Amorim VM, de Almeida Ferrari AS, de Souza AS, Guzzo CR. 2025 Latin America's dengue outbreak poses global health threat. *Viruses* **17**, 57. (doi:10.20944/preprints202407.0405.v2)
78. Xu C, Xu J, Wang L. 2024 Long-term effects of climate factors on dengue fever over a 40-year period. *BMC Public Health* **24**, 1451. (doi:10.1186/s12889-024-18869-0)

Downloaded from royalsocietypublishing.org/rsif/article-pdf/doi/10.1098/rsif.2026.0438/6159915/rsif.2026.0438.pdf
by guest
on 05 November 2026

79. Borges IVG *et al.* 2025 Analysis of the interrelationship between precipitation and confirmed dengue cases in the city of Recife (Brazil) covering climate and public health information. *Front. Public Health* **12**, 1456043. (doi:10.3389/fpubh.2024.1456043)
80. Couret J, Benedict MQ. 2014 A meta-analysis of the factors influencing development rate variation in *Aedes aegypti* (Diptera: Culicidae). *BMC Ecol.* **14**, 3. (doi:10.1186/1472-6785-14-3)
81. Stewart Ibarra AM, Ryan SJ, Beltrán E, Mejía R, Silva M, Muñoz A. 2013 Dengue vector dynamics (*Aedes aegypti*) influenced by climate and social factors in Ecuador: implications for targeted control. *PLoS ONE* **8**, e78263. (doi:10.1371/journal.pone.0078263)
82. Lowe R, Stewart-Ibarra AM, Petrova D, García-Díez M, Borbor-Cordova MJ, Mejía R, Regato M, Rodó X. 2017 Climate services for health: predicting the evolution of the 2016 dengue season in Machala, Ecuador. *Lancet Planetary Health* **1**, e142–e151. (doi:10.1016/s2542-5196(17)30064-5)
83. Gabrick EC. 2026 Climate change modulates dengue synchronization. Zenodo. (doi:10.5281/zenodo.20630673)

Downloaded from royalsocietypublishing.org/rsif/article-pdf/doi/10.1098/rsif.2026.0438/6159915/rsif.2026.0438.pdf
by guest
on 05 November 2026